PalArch's Journal of Archaeology of Egypt / Egyptology

SPEED CONTROL OF A BDFRM DRIVE BY USING MODEL PERIDECTIVE CURRENT CONTROL TECHNIQUE

P. A. Prabhakara[1], S. Shridhar[2], A.Aruna[3]

[1] Assistant Professor (Adhoc), JNTUA College of Engineering, Anantapur.

[2] Assistant Professor, JNTUA College of Engineering, Anantapur.

[3]Post Graduate Student, JNTUA College of Engineering, Anantapur.

P. A. Prabhakara , S. Shridhar , A.Aruna , Speed Control Of A Bdfrm Drive By Using Model Peridective Current Control Technique , Palarch's Journal Of Archaeology Of Egypt/Egyptology 18(10), 1893-1913. ISSN 1567-214x.

ABSTRACT

Model predictive control (MPC) is now considered an effective control approach for achieving accurate and rapid drive control. Model predictive control the voltage vectors needs to assessed in control objectives defined in terms of power, current, flux, andtorque. An iterative prediction loop, for choosing the best optimal one for the following control interval. Easy to implement Model Predictive Control and shows obvious unique execution, but in the steady state performance is hampered to thevoltage vectors areavailable in limited range, mainly in two-level voltage-source-inverters.The purpose of this project is to investigate the viability of the Model predictive control approach for a fresh student, a BDFRM drive, using thecontrol variable is secondary current. In addition, the duty-cycle control approach is used to address the issue of steady-state inferiorityBy replacing the inner current proportional-integral (PI) controllers and pulse-width modulator with an optimization-based model predictive current controller. In contrast to the suggested work, extensive MATLAB simulation analysis was performed.

NOMENCLATURE

R_p, R_sResistance for Primary and secondary winding (Ω)

L_p, L_s, L_{ps}Self-and mutual inductances (H)

v, i, λ Voltage (V), current (A), and flux linkages (Wb-t) vectors

$\omega_{p,}\omega_s$Angular frequency(rad\s) of primary and secondary voltage\ current

ω_p, ω_{rm}, N_r Electrical and mechanical angular speed of rotor in (rad\s) and number of revolution per minute (rpm)

θ_r Angular position (rad) of rotor

p_p, p_s, p_r Primary, secondary and rotor poles

θ_p , θ_s Primary and secondary reference frame position (rad)

P_p, Q_pPrimary active (W) and reactive (VAr) Power

k Discrete time index

Super-script

r, s Rotating and stationary frame quantities

ref Reference value of a variable

Sub-script

p, s Primary and secondary variables

d, q Direct- and quadrature-components of a variable

a, b, c Phase quantities

INTRODUCTION

BDFMs may effectively replace wound rotor induction machines and singly-fed machines in variable-speed consistent recurrence age frameworks and variable recurrence speed regulation of machine[1] due to the economic benefits of fractionally-rated converters.The chance of utilizing minimal expense partially evaluated inverter for applications with a restricted speed range, further developed dependability of brushless rotor [2], extra complex method activities, crowbarless low voltage ride-through (LVRT) matrix joining ability, particular benefits to challenge with the traditional decisions [1]. In the group of brushless doubly-fed machines has two arrangements of electrically autonomous stator three-stage windings imparting normal attractive circuit to the rotor inclusion. At power recurrence, the associationof primary winding is straightforwardly to a consistent three-stage ac power supply.To obtain the appropriate speed, the frequency of secondary winding is adjusted by a bidirectional rectifier [3]. Furthermore, the pole designs for both windings are different [4], [5]. Different formsof doubly-fedbrushlessmachine topologies with different rotor configurations, including as cage rotors, reluctance rotors, wrapped rotors, hybrid rotors, and so on, have been intensively investigated in recent decades. [5] lists the properties of these rotor structures as well as some illustrative references.In Brushless doubly-fed machines, two basic types of rotor architectures are used: reluctance and cage rotors.

In off-shore settings where rotor access is restricted, the brushless doubly-fed machine drive with reluctance rotor is easier to model and operate, as well as more robust and dependable. Furthermore, because the brushless doubly-fed reluctance machine (BDFRM) lacks a rotor circuit and current, it has a smaller saturation effect and is more efficient than a brushless doubly-fed induction machine (BDFIM). In terms of starting and asynchronous

characteristics, BDFIM surpasses BDFRM, while BDFRM outperforms BDFIM in terms of simultaneous activity and customizable doubly-fed speedexecution [6].

In the doubly-fed brushless reluctance machine literature, scalar control (SC) [7], and direct torque control (DTC) [10] techniques are well-established control methodologies.An amplitude andrecurrence of the regulating parameters are correspondingly modified in the Scalar control approach to keep the flux constant.The method provides a straightforward option for applications with a limited speed range where great performance is not necessary [7].Vector control/Field oriented control, on the other hand, can provide quick, exact, and effective control of thedoubly-fed brushless reluctance machine drive.The technique must be implemented in a rotating reference frame.The method provides a straightforward option for applications with a limited speed range where great performance is not necessary [7]. Vector control or Field oriented control, on the other hand, can provide quick, exact, and effective control of the brushless doubly-fed reluctance machine drive.The technique must be implemented in a rotating reference outline. The switching pulses for the rectifier are produced by a pulse width modulator (PWM) and at least three PI regulators [13].The cascaded structure of current andspeed controllers limits the bandwidth of operation and control rate. In addition, tweaking of PI regulators is needed for the steady activity of the drive framework over the whole control range.

In spite ofField oriented control/Vector control, Direct torque control approach can handle the flux and torque straightforwardly with quick and precise elements utilizing unassuming construction. PI controllers to be implemented.The method is appropriate for applications demanding high dynamic responsiveness due to the direct pulse generating strategy. The main disadvantages of direct torque control are thelarge currentripples,

Model predictive control (MPC) method has considered as a leading approach due to the emergence of improved control hardware platforms. As a result, in recent decades, the many control elements of this technique have been the focus of extensive investigation for various machine drive control.The discrete model of the system is primarily used in Model Predictive Control to estimate future behaviour of controllable variables such as power [18], torque,current [15], and flux, among others [17]. If used properly, the technique may deal with numerous restrictions like as switching frequency minimization,overcurrent protection, and so on in naturally [17]. It also allows for the operation of a discrete power electronic converter with a limited number of switching stages and a sample-based digital signal processor (DSP).]..The Model predictive power controland Model predictive current control algorithms are easier to implement than Model predictive torque control because they only consider one type of variable (power orcurrent error) in the objective function, which is divided into real and imaginary components.Furthermore, in Model predictive torque control, the linear combination of flux and torque errors must be decreased equally, requiring weighting factor tuning to account for changes in the physical nature, magnitudes, and units of the variables [22]

During the whole control period, the conventional Model predictive current control method traditional single-vector-based Model predictive current control can be improved, similar to Direct torque control [14]. Based on this analysis, the present study combines the theory of duty-cycle control by employing a single zero voltage vector in conjunction with an optimal active voltage vector calculatedusing a typicalModel predictive current control algorithm during one control period.Furthermore, hardware time delay is modified using two-step prediction to improve control precision.Computer simulations in MATLAB/Simulink are used to validate the proposed Model predictive current control approach. The drive's resistance to parameter fluctuations is also assessed.

II. THEORETICAL DEVELOPMENT OF THE MODEL PREDICTIVE CURRENT CONTROL FOR DOUBLY-FED BRUSHLESS RELUCTANCE MACHINE DRIVE SPEED CONTROL

The controller was built using the stationary frame machine paradigm to reduce computing complexity and avoid the challenges of inverter voltage vector position transformations. The basic field oriented control method for the doubly-fed brushless reluctance machine drive control in this project is based on the machine's essential characteristics as mentioned in [8], [13].

The first and second voltages of doubly-fed brushless reluctance machine are given by the dynamic equations [4].

$$v^s_{pd}=R_p i^s_{pd}+d\lambda^s_{pd}/dt-\omega_p\lambda^s_{pq} \quad (1)$$

$$v^s_{pq}=R_p i^s_{pq}+d\lambda^s_{pq}/dt+\omega_p\lambda^s_{pq} \quad (2)$$

$$v^s_{sd}=R_s i^s_{sd}+d\lambda^s_{sd}/dt-\omega_s\lambda^s_{sq} \quad (3)$$

$$v^s_{sq}=R_s i^s_{sq}+d\lambda^s_{sq}/dt+\omega_s\lambda^s_{sq} \quad (4)$$

where,

$$\lambda^s_{pd}=L_p i^s_{pd} + L_{ps}\cos\theta_r i^s_{sd} + L_{ps}\sin\theta_r\, i^s_{sq} \quad (5)$$

$$\lambda^s_{pq}=L_p i^s_{pq} + L_{ps}\sin\theta_r i^s_{sd} - L_{ps}\cos\theta_r\, i^s_{sq} \quad (6)$$

$$\lambda^s_{sd}=L_s i^s_{sd} + L_{ps}\cos\theta_r i^s_{pd} + L_{ps}\sin\theta_r\, i^s_{pq} \quad (7)$$

$$\lambda^s_{sq}=L_s i^s_{sq} + L_{ps}\sin\theta_r i^s_{pd} - L_{ps}\cos\theta_r\, i^s_{pq} \quad (8)$$

The proposed MPCC approach is used to control the speed of the BDFRM drive in Figure 1. The system is mostly made up of secondary current estimate and secondaryreference frame position, as well as the formation of a secondary reference current, and MPCC controller is used to control the current.

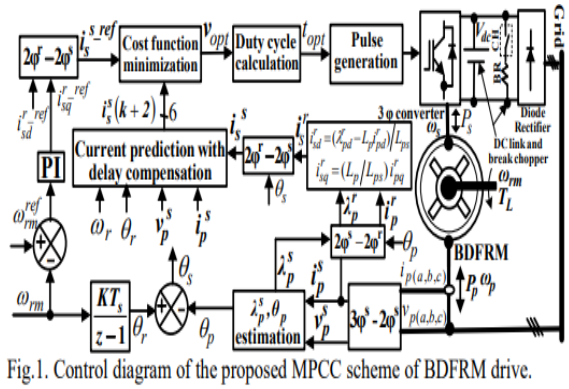

Fig.1. Control diagram of the proposed MPCC scheme of BDFRM drive.

A. Position of the Secondary Reference Frame and Secondary Current Estimation

The secondary current components and their references must be converted into stationary equivalents since the rest of the control algorithm is developed in a stationary reference frame. As a result, the secondary frame position (θ_s) must be established. The primary

reference frame position in the Primary field oriented control condition is the location of the primary winding flux with respect to the stationary reference frame(θ_p), which is utilised to calculate ofθ_s[8].

$\lambda_p^s=\int(v_p^s-R_s i_p^s)dt$(9)

$\theta_p = \tan^{-1}\left(\lambda_{pq}^s/\lambda_{pd}^s\right)$(10)

$\theta_p = \theta_r - \theta_p$(11)

The secondary current is estimated using primary variables to reduce the number of current sensors and increase the quality of secondary current waveforms.

$i_{sd}^r = \left(\lambda_{pd}^r - L_p i_{pd}^r\right)/L_{ps}$ (12)

$i_{sq}^r = \left(L_p/L_{ps}\right)i_{pq}^r$(13)

B. Secondary Sources Current Generation

TheRotor reference speed is compared to speed criticism. Furthermore, the speed complaint is contrasted with the reference speed, and the error is taken care of. In addition, a PI regulator is used to produce the q-axis auxiliary current reference (i_{sq}^{ref}) in the ω_s rotating reference outline. For decoupled speed/torque and flux control, the d-axis current reference (i_{sd}^{ref}) is kept constant. Furthermore, it is set to zero in order to get the greatest torque per inverter ampere (MTPIA) [8]

C. Model Predictive Current Control controller is used to control the current.

The recommended current controller system is primarily intended for secondary current predictions with delay time remuneration corresponding to inverter active voltage vectors, optimal active voltage vector selection via objective function minimization, active voltage vector duty-cycle computation, and switching state selection for 2L-VSI

1) Prediction of current taking compensation for delay time.

Due to the refreshing system of DSPs and microcontrollers, the regulator output at k^{th} period cannot be applied in a flash at $(k+1)^{th}$ period during the computerised execution of Model Predictive Current Control. To achieve better prediction, one-venture delay is remunerated using two-venture expectation [29]. In order to compensate for delays, the first-step prediction is used.

$di_{sd}^s/dt = (1/a)$

$$\begin{Bmatrix} v_{sd}^s - bv_{pd}^s - cv_{pq}^s + di_{pd}^s \\ -ei_{pq}^s - R_s i_{sd}^s + fi_{sq}^s \end{Bmatrix} (14)$$

$di_{sq}^s/dt=(1/a)$

$$\begin{Bmatrix} v_{sq}^s - cv_{pd}^s - bv_{pq}^s - ei_{pd}^s \\ -di_{pq}^s - R_s i_{sq}^s - fi_{sd}^s \end{Bmatrix} \qquad (15)$$

where,

$$\left.\begin{aligned} a &= \sigma L_s \\ b &= \left(L_{ps}\cos\theta_r\right)/L_p \\ c &= \left(L_{ps}\sin\theta_r\right)/L_p \\ d &= \left(\omega_r L_p L_{ps}\sin\theta_r + R_p L_{ps}\cos\theta_r\right)/L_p \\ e &= \left(\omega_r L_p L_{ps}\cos\theta_r - R_p L_{ps}\sin\theta_r\right)/L_p \\ f &= L_s\left(\omega_r - \sigma\omega_p\right), \sigma = 1 - L_{ps}^2/\left(L_p L_s\right) \end{aligned}\right\} (16\text{For}$$

The technique is divided into two phases: forecasting and rectification. The results of the anticipation stage are the predicted optional flows obtained by Euler's first-request discretization. Let, them be referred to as $i^{s*}_{sd}(k+1)$ and $i^{s*}_{sq}(k+1)$ separately where,

$$i^{s*}_{sd}(k+1)=i^{s}_{sd}(k)\left(\frac{T_s}{a}\right) \begin{Bmatrix} v^{s}_{sd}(k) - bv^{s}_{pd}(k) - cv^{s}_{pq}(k) + di^{s}_{pd}(k) \\ -ei^{s}_{pq}(k) - R_s i^{s}_{sd}(k) + fi^{s}_{sq}(k) \end{Bmatrix} \quad (17)$$

$$i^{s*}_{sq}(k+1)=i^{s}_{sq}(k)\left(\frac{T_s}{a}\right) \begin{Bmatrix} v^{s}_{sq}(k) - cv^{s}_{pd}(k) + bv^{s}_{pq}(k) - ei^{s}_{pd}(k) \\ -di^{s}_{pq}(k) - R_s i^{s}_{sq}(k) - fi^{s}_{sd}(k) \end{Bmatrix} \quad (18)$$

Thus, (17)- (18) are utilized as the indicators of the optional flows. Moreover, $i^{s*}_{sd}(k+1)$and$i^{s*}_{sq}(k+1)$ are used to make more accurate final forecastsof $i^{s}_{sd}(k+1)$ also $i^{s}_{sq}(k+1)$, as

$$i^{s}_{sd}(k+1)=i^{s}_{sd}(k)\left(\frac{T_s}{a}\right) \begin{bmatrix} v^{s}_{sd}(k) - bv^{s}_{pd}(k) - cv^{s}_{pq}(k) + di^{s}_{pd}(k) - ei^{s}_{pq}(k) \\ -R_s\left\{\frac{i^{s}_{sd}(k) + i^{s*}_{sd}(k+1)}{2}\right\} + f\left\{\frac{i^{s}_{sq}(k) + i^{s*}_{sq}(k+1)}{2}\right\} \end{bmatrix} (19)$$

$$i^{s}_{sq}(k+1)=i^{s}_{sq}(k)\left(\frac{T_s}{a}\right) \begin{bmatrix} v^{s}_{sq}(k) - cv^{s}_{pd}(k) + bv^{s}_{pq}(k) - ei^{s}_{pd}(k) - di^{s}_{pq}(k) \\ -R_s\left\{\frac{i^{s}_{sq}(k) + i^{s*}_{sq}(k+1)}{2}\right\} - f\left\{\frac{i^{s}_{sd}(k) + i^{s*}_{sd}(k+1)}{2}\right\} \end{bmatrix} (20)$$

Conditions (19)- (20) can additionally be simplified as

$$i^{s}_{sd}(k+1)=i^{s*}_{sd}(k+1)\left(\frac{T_s}{a}\right) \begin{bmatrix} -R_s\left\{i^{s*}_{sd}(k+1) - i^{s*}_{sd}(k)\right\} \\ +f\left\{i^{s*}_{sq}(k+1) - i^{s*}_{sq}(k)\right\} \end{bmatrix} \quad (21)$$

$$i^{s}_{sq}(k+1)=i^{s*}_{sq}(k+1)\left(\frac{T_s}{a}\right) \begin{bmatrix} -R_s\left\{i^{s*}_{sq}(k+1) - i^{s*}_{sq}(k)\right\} \\ +f\left\{i^{s*}_{sd}(k+1) - i^{s*}_{sd}(k)\right\} \end{bmatrix} \quad (21)$$

The second-stage of expectations i.e., estimation of$i^{s}_{sd}(k+2)$ and $i^{s}_{sq}(k+2)$.

2) Objective function minimization

Because different voltage vectors produce distinct current fluctuations, it is important to consider each voltage vector's effect independently and choose the optimum one that

minimises current inaccuracy. The assessment is made in terms of an objective function, which is written as

$$g_x = \left|i_{sd}^{s\_ref} - i_{sd}^{s}(k+2)\right|^2 + \left|i_{sq}^{s\_ref} - i_{sq}^{s}(k+2)\right|^2\Big|_{x=1:6} \quad (23)$$

Six dynamic vectors are used in the computation of target work. The default one is saved as g_{opt}. One of the two zero voltage vectors is used for the rest of the control stretch.

3) Determination of the duty cycle

For a small portion of the control time, the ideal dynamic voltage vector is used. Zero vectors, on the whole, cause in each of the six stages, two sets of inclines should be determined. Individually, the present inclines caused by the ideal dynamic vectorv_{opt} and the zero vector v_0 are (s_{1d}, s_{1q}) and(s_{0d}, s_{0q}), respectively.

$$s_{0d} = \frac{di_{sd}^{s}}{dt}\Big|_{v_{sd}^{s}=v_{0d}} = \left(\frac{1}{a}\right)\begin{Bmatrix} -bv_{pd}^{s} - cv_{pq}^{s} + di_{pd}^{s} \\ -ei_{pq}^{s} - R_s i_{sd}^{s} + fi_{sq}^{s} \end{Bmatrix} \quad (24)$$

$$s_{1d} = \frac{di_{sd}^{s}}{dt}\Big|_{v_{sd}^{s}=v_{opt\_d}} = s_{0d} + \left(\frac{1}{a}\right) v_{opt\_d} \quad (25)$$

$$s_{0q} = \frac{di_{sq}^{s}}{dt}\Big|_{v_{sq}^{s}=v_{0q}} = \left(\frac{1}{a}\right)\begin{Bmatrix} -cv_{pd}^{s} + bv_{pq}^{s} - ei_{pd}^{s} \\ -di_{pq}^{s} - R_s i_{sq}^{s} - fi_{sd}^{s} \end{Bmatrix} \quad (26)$$

$$s_{1q} = \frac{di_{sq}^{s}}{dt}\Big|_{v_{sq}^{s}=v_{opt\_q}} = s_{0q} + \left(\frac{1}{a}\right) v_{opt_q\_q} \quad (27)$$

At long last, the anticipated current parts at moment k+2 is calculated as

$$i_{sd}^{s}(k+2) = i_{sd}^{s}(k+1) + s_{1d}t_{opt} + s_{0d}(T_s - t_{opt}) \quad (28)$$

$$i_{sq}^{s}(k+2) = i_{sq}^{s}(k+1) + s_{1q}t_{opt} + s_{0q}(T_s - t_{opt}) \quad (29)$$

The ideal length (t_{opt}) of the best dynamic vector during one test cycle fulfils the accompanying condition

$$\frac{\partial g_{opt}}{\partial t_{opt}} = 0 \quad (30)$$

Subbing (28), (29) in (23) and in this way utilizing (30), t_{opt} not really set in stone as

$$t_{opt} = \frac{T_s\begin{pmatrix} {s_{0d}}^2 - s_{0d}s_{1d} \\ -s_{0q}s_{1q} + {s_{0q}}^2 \end{pmatrix} + \begin{bmatrix} (s_{1d} - s_{0d})\{i_{sd}^{s\_ref} - i_{sd}^{s}(k+1)\} \\ +(s_{1q} - s_{0q})\{i_{sq}^{s\_ref} - i_{sq}^{s}(k+1)\} \end{bmatrix}}{(s_{0d} - s_{1d})^2 + (s_{0q} - s_{1q})^2} \quad (31)$$

where,

$$t_{opt} = \begin{cases} 0, & \text{if} t_{opt} > T_s \\ T_s, & \text{if} t_{opt} > T_s \end{cases} \quad (32)$$

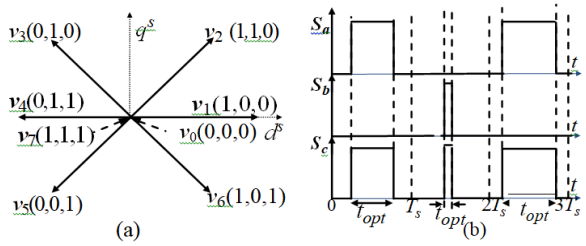

Fig.2. Inverter exchanging: (a) 2L-VSIVoltage vectors, and (b) Duty-cycleEstimationusingSwitching in MPCC.

4) Switching state selection for 2L-VSI

In Fig.2(a) and Fig.2(b), the voltage vectors of 2L-VSI are compared to their exchanging states, and the exchanging examples of MPCC with duty-cycle control are shown separately. [17] gives the voltage vector size in comparison to its exchanging state (see Table 4.2 in that). For ideal time length(t_{opt}), the ideal voltage vector among six dynamic vectors($v_{1:6}$) is used, as shown in Fig.2(b). The magnitude of the applied voltage vector adapts just when duty-cycle improves, and its path remains unchanged. In the remaining time span.($T_s - t_{opt}$), the zero voltage vector ($v_{0/7}$) is used, which needs the least number of exchanging advances.The following is a summary of the above-mentioned current control technique's calculation:

1. Estimation of v_p^s,i_p^s ,ω_{rm};

2. Assessment ofλ_p^s,i_s^s,θ_p,θ_s,θ_r;

3. Estimation of $i_{sd}^{s\_ref}$,$i_{sq}^{s\_ref}$;

4. First stage forecast ofi_s^s (21)- (22)

$$i_s^s(k+1) = f_1\{i_p^s, i_p^s(k), i_s^s(k), v_{opt}\};$$

5. for x=1:6, Duty-cycle determination (31)

$$t_{opt\_x} = f_2\{i_s^s(k+1), i_s^{s\_ref}(k+1), s_{1\_x}, s_0\};$$

6. Second stage forecast ofi_s^s(28)- (29)

$$i_s^s(k+2) = f_3\{i_s^s(k+1), s_{1\_x}, s_0 t_{opt\_x}\};$$

7. Estimation of target work (23)

$$g_x = f_4\{i_s^{s\_ref}, i_{sd}^s(k+2)\};$$

8. If g_x>=g, go to stage 10;

9. elseg_{opt}=g_x,$v_{opt} = v_x$,$s_1 = s_{1\_x}$, $t_{opt} = t_{opt\_x}$;

10. Augmentation of x by 1;

11. assuming(x<6), go to stage 5;

12. Utilization of exchanging states relating tov_{opt},$v_0$fort_{opt},($T_s - t_{opt}$) stretch separately;

III. RESULTS OFSIMULATION AND EXTENSION

An exhibition of the suggested control plot has been researched broadly for 30 % of speed varieties around coordinated speed recreations in MATAB/Simulink. The machine determinations are introduced in APPENDIX A (see TABLE IV).

A. Simulation Results

In this section, couple simulation results are shown to demonstrate the drive execution for the recommended model predictive current control approach in motoring and generating modes for the constant-torque variable-speed motion.

At 9 Nm load torque, Fig.3 shows the motor execution in the motoring manner of activity. The As demonstrated in Fig. 3, the rotor speed tracks the reference speed flawlessly throughout the speed control range (a). In full speed runs, the overall speed blunder is under 10 rpm in a steady condition, and only floods up to 20 rpm during speed drifters, as shown in Fig.3 (b). Figure 3 depicts the torque profile (c).During the transitory phase, the electromagnetic torque works perfectly, and there is an acceptable amount of waves everywhere. The decoupling i_{sd}^{r} and i_{sq}^{r} inFig.3(d) indicate that the Primary field oriented control condition is viable. Under constant load torque conditions, the size of i_{sq}^{r} is essentially constant for all working speeds. Furthermore, using the Maximum torque per inverter ampere driving mechanism,i_{sd}^{r} remains zero throughout. It can be observed in Fig.3(e) that i_{sd}^{s}follows its reference $i_{sd}^{s\_ref}$ to the point. i_{sd}^{s} and i_{sq}^{s} are exhibited at super-synchronous speed in Fig.3(f).The current frequencies remain the same for the same measure of speed variation from super-simultaneous to sub-coordinated speed, but the stage succession inverts.

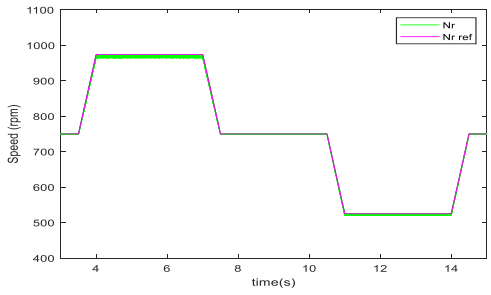

(a)

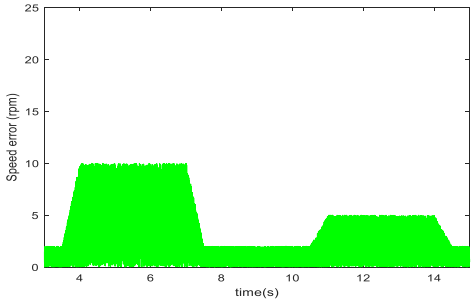

(b)

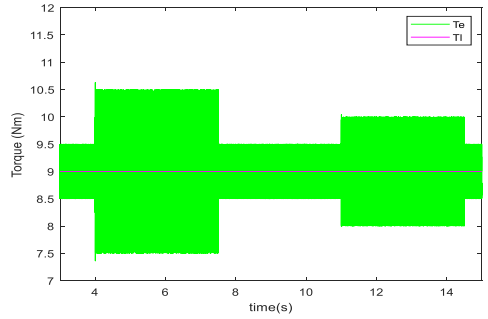

(c)

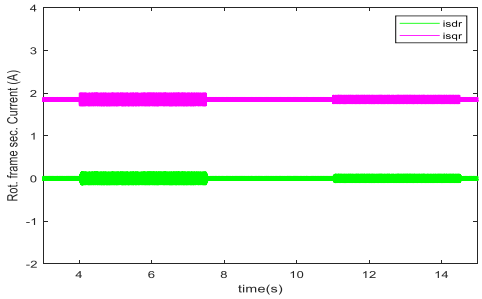

(d)

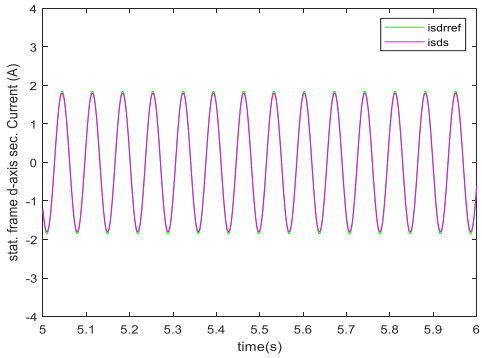

(e)

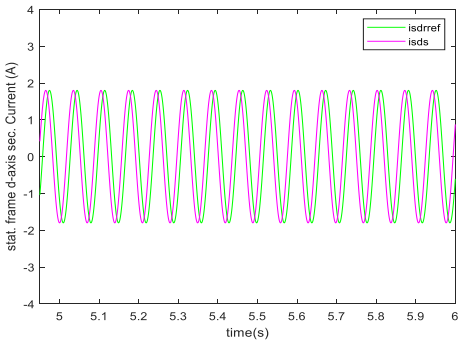

(f)

Fig.3. Simulation results-1:Under Model Predictive (a) Speed following execution, (b) Absolute speed mistake, (c) Torque designs, (d) Rotating outline auxiliary current , (e) Stationary edge d-pivot auxiliary current reference following, and (f) Stationary edge auxiliary currents.

Figure 4 shows the variable speed execution in the drive's generating approach. The machine's speed tracks the reference speed unequivocally during activity, as seen in Fig.4(a).In simultaneous and super-synchronous speed ranges, the amplitude of supreme speed error is less than 5 rpm, but it varies between 10 rpm and 20 rpm in sub-coordinated

speed ranges. At 9 Nm shaft torque, Fig.4(c) depicts the important active and reactive power profiles. As can be observed from the i sdr and i sqr waveforms in Fig.4(d), the Primary field oriented control and Maximum Torque Per Inverter Ampere criteria are met in this scenario.Fig.4(e) and Fig.4(f) show thati_{sd}^{s} follows$i_{sd}^{s_ref}$ agreeably Furthermore, in the super-simultaneous speed area, it is 90 degrees ahead of i_{sq}^{s}. At 415 V, the fundamental winding is connected to the framework (see Fig.4(g)). The optional voltage, however, is determined by the constant DC interface voltage and the exchanging state vector (see Fig.4(h)).

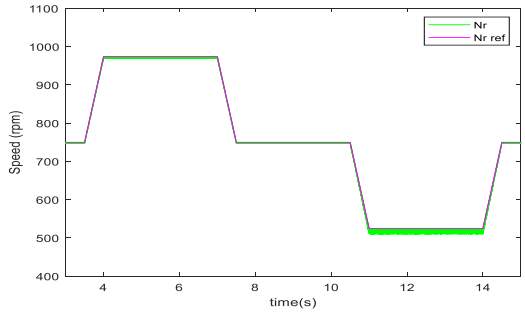

a.

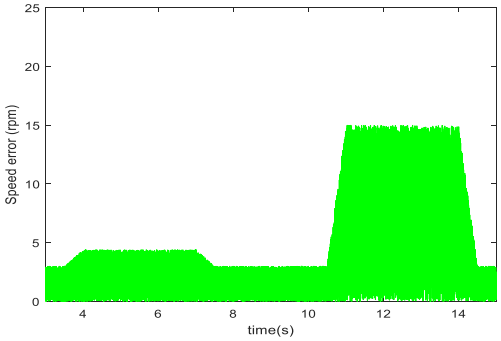

b.

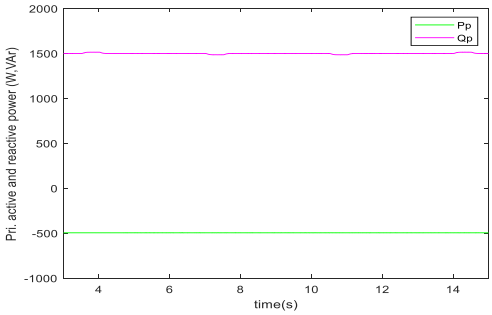

c.

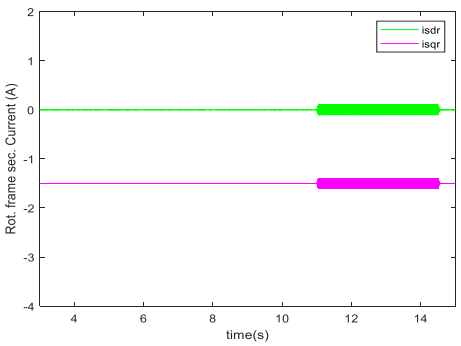

d.

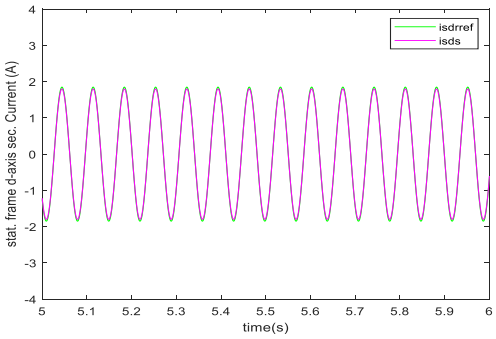
isdrref
isds
stat. frame d-axis sec. Current (A)
time(s)

e.

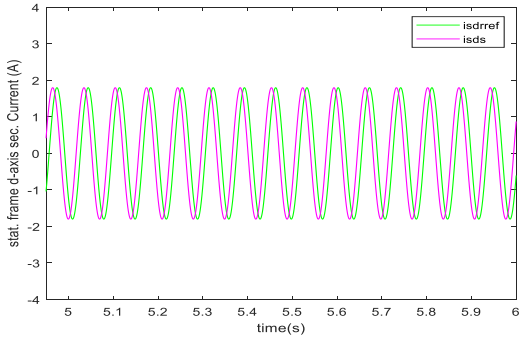
isdrref
isds
stat. frame d-axis sec. Current (A)
time(s)

f.

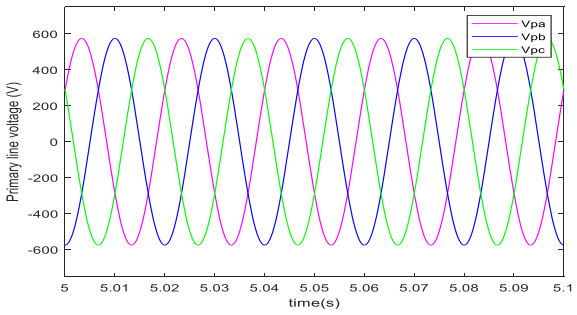
Vpa
Vpb
Vpc
Primary line voltage (V)
time(s)

g.

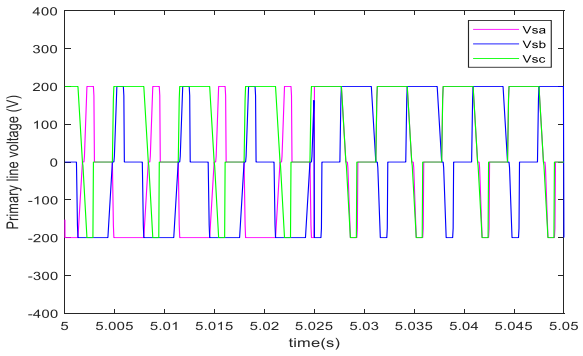
Vsa
Vsb
Vsc
Primary line voltage (V)
time(s)

h.

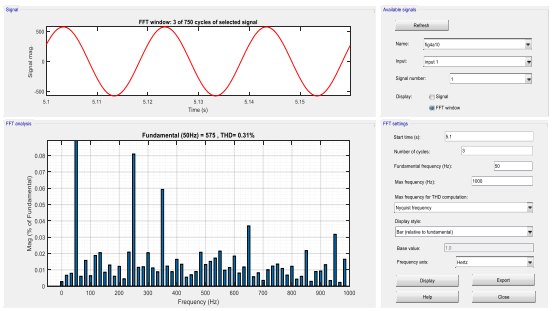

i

Fig.4. Simulation results-2: Variable-speed (750-974-750-525 rpm) and consistent torque (- 9 Nm/ - 0.5 pu producing mode) activity under MPCC plot: (a) Speed following execution, (b) Absolute speed mistake, (c) Primary power, (d) Rotating outline auxiliary current, (e) Stationary edge d-pivot auxiliary current reference following, (f) Stationary edge auxiliary current, (g) Primary line voltages, and (h) Secondary line voltages,(i)THD

B. Extension results

Simulation results using anfis controller:

Load torque at 9NM:

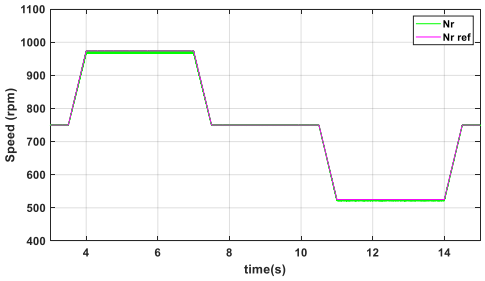

(a) Speed tracking performance

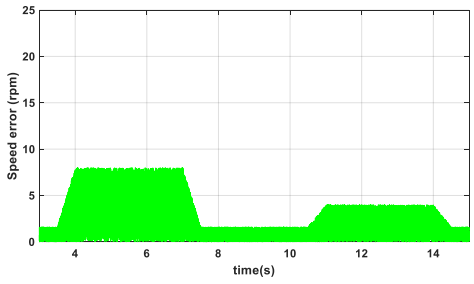

(b) Absolute speed error

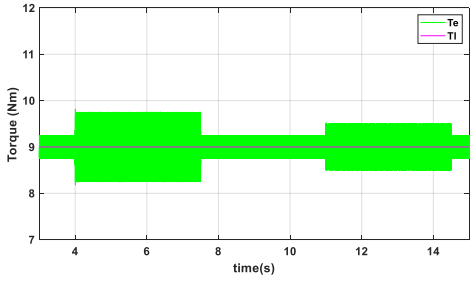

(c) Torque patterns

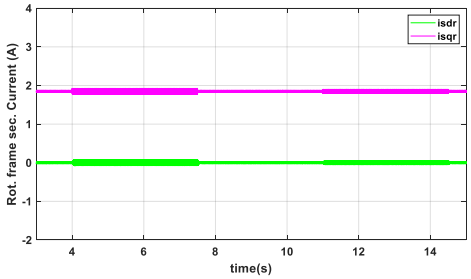

(d) Rotating frame secondary currents

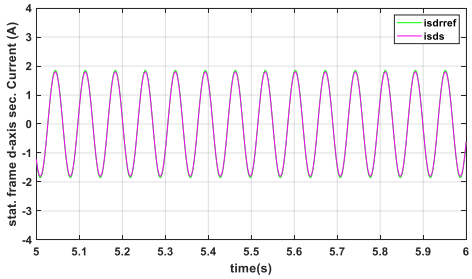

(e) Stationary frame d-axis secondary current reference tracking

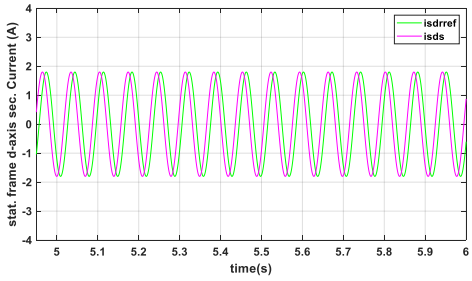

(f) Stationary frame secondary currents

Load torque at -9NM:

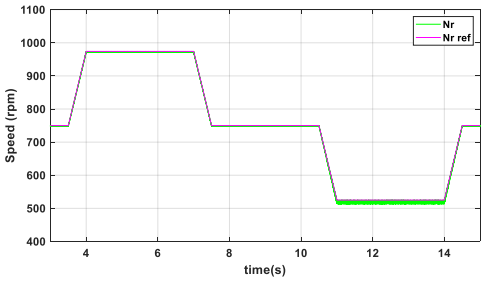

(a) Speed tracking performance

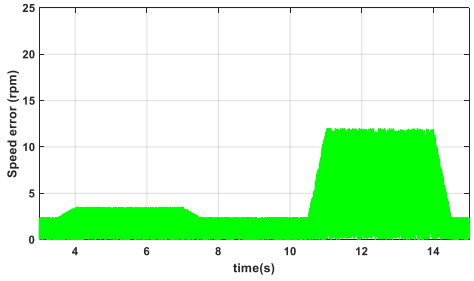

(b) Absolute speed error

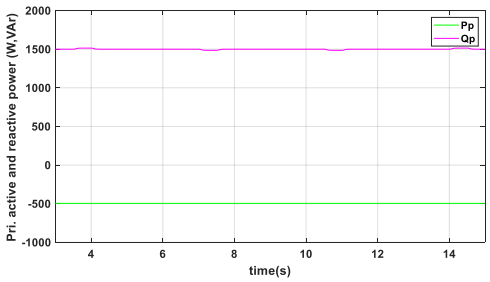

(c) Primary power

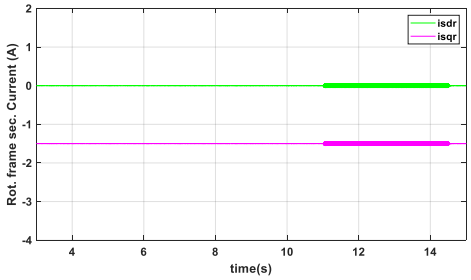

(d) Rotating frame secondary currents

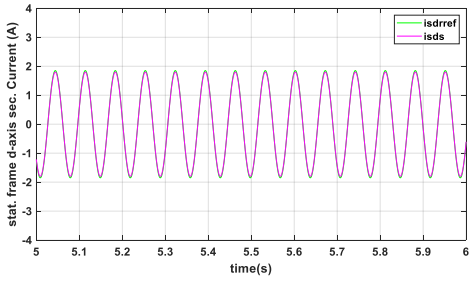

(e) Stationary frame d-axis secondary current reference tracking

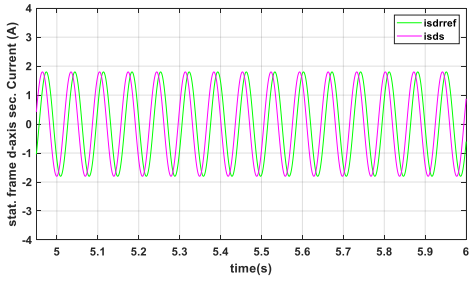

(f) Stationary frame secondary currents

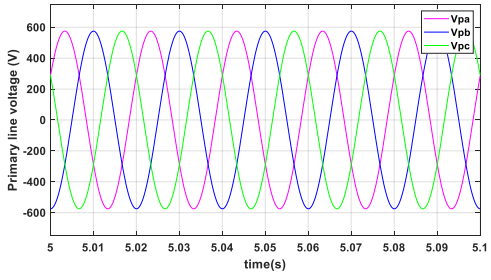

(g) Primary line voltages

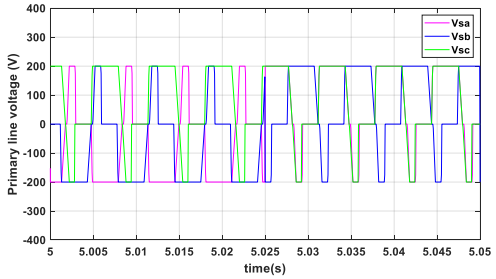

(h) Secondary line voltage

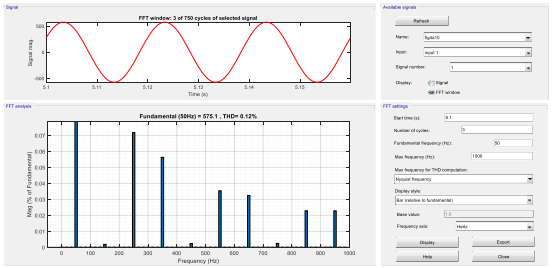

(i)THD

The Total Harmonic Distortion values for PI and ANFIS controllers are given below

	PI controller	ANFIS controller
THD	0.31%	0.12%

V. CONCLUSION

The field-oriented speed management of a brushless doubly fed reluctance machine drive is presented in this project using a model predictive current control procedure.The model predictive current control regulator includes the idea of duty-cycle regulation to expand the amount of opportunity for 2L-VSI swapping territories.Under that regard, a ZVV is distributed in the regulation calculation for a small part of monitoring interval alongside an ideal DVV, since, it creates the littlest variation in regulation factors. The optimal length for using the active and ZVV is found by subtracting related current slants.

The plan is tentatively approved in regulating and producing systems for speed regulation of brushless doubly fed reluctance machine drivethe general benefits in the presented conspire on customary field-oriented control plot are stressed. The strategy has important advantages over field-oriented control, such as a good powerful condition with fewer swapping losses.The following are the components of the suggested method's strategy.

- The model predictive current control regulator plot is undifferentiated from field-oriented control since auxiliary current is employed as a controlling parameter.
- The computation in the fixed variable outline takes fewer axis changes to complete.
- Lacking of internal current Proportional integral regulators minimizing the rushed adjusting of Proportional integral regulator enhancement,expands bandwidth of working locales and works on the powerful execution of the drive framework.

- The application of a discontinuous framework model for the inverter's direct age of exchanging circumstances prevents any PWM from contributing, resulting in a reduction in execution difficulty.
- Following execution, a secondary current blunder platform that offers improvement calculation ascribes tremendous speed.
- Incorporation of the duty-cycle concept into the regulation calculation further develops consistent state execution of the drive framework by diminishing current waves.

Like the regular model predictive current control's techniques, the association of the specification-based target work assessment joined the duty-cycle estimate grows even more. the calculation interaction of the presently used methodology. Thus, the effective processor is additionally required for its on-going execution.

TABLE IV
FOR THE SUGGESTED WORK, MACHINE CONFIGURATIONS

Brushless Doubly Fed Reluctance Machine rating		**Direct Current machine rating**	
Rated power	1.6 kW	Rated power	1.5 kW
Current	3/ 2.3 A	Rated current	8 A
Line voltage	415/415 V	Rated voltage	220 V
Primary supply frequency	50 Hz	Rated speed	1500 rpm
No. of rotor, primary and secondary poles	4, 6, 2	Type	Separately - excited
Primary and secondary winding resistances	10.2 Ω, 12.8 Ω	Duty	CMR (S1)
Primary and secondary winding self-inductances	0.38 H, 0.54 H		
Primary and secondary winding mutual inductance	0.32 H		
Rotor inertia	0.035 kg m^2		
Friction coefficient	0.0014		

Likewise, the standard of miscreant regulationwill be accepted to handle regulation intricacy and the weight of analysis. In addition, the regulator execution despite system boundary varieties will be settled with reasonable assessment methods.

REFERENCES

[1] P.Han, M.Cheng, S.Ademi and M.Jovanovic, "Brushless doubly-fed machines: opportunities and challenges," Chinese Journal of Electrical Engineering , vol. 4, no. 2, pp. 1-17, June 2018.

[2] S.Abdi, E.Abdi and R.McMahon, "A light-weight rotor design for brushless doubly fed machines," in Proc. International Conference on Electrical Machines (ICEM), Alexandroupoli, Greece, 3-6 Sept. 2018.

[3] R.Cárdenas, R.Pena, S.Alepuz and G.Asher, "Overview of control systems for the operation of DFIGs in wind energy applications," IEEE Trans. Ind. Electron., vol. 60, no. 7, pp. 2776-2798, July 2013.

[4] R.Betz and M.Jovanovic, "Introduction to brushless doubly fed reluctance machines- the basic equations," Aalborg University, Aalborg, Denmark, March2012.

[5] M.Jovanovic, R.Betz and J.Yu, "The use of doubly fed reluctance machines for large pumps and wind turbines," IEEE Trans. Ind. Appl., vol. 38, no. 6, pp. 1508-1516, 2002.

[6] S.Ademi and M.Jovanovic, "Vector control methods for brushless doubly-fed reluctance machines," IEEE Trans. Ind. Electron., vol. 62, no. 1, pp. 96-104, Jan.2015.

[7] M.Jovanovic, "Sensored and sensorless speed control methods for brushless doubly fed reluctance motor," IET Electric Power Applications, vol. 3, no. 6, pp. 503-513, Nov.2009.

[8] H.Chaal and M.Jovanovic, "Direct power control of brushless doubly-fed reluctance machines," in Proc. IET International Conference on Power Electronics, Machines and Drives (PEMD), Brighton, UK, 19-21 April 2010.

[9] L.Xu, L.Zhen and E.Kim, "Field-orientation control of a doubly excited brushless reluctance machine," IEEE Trans. Ind. Appl., vol. 34, no. 1, pp. 148-155, Jan./Feb. 1998.

[10] K.Kiran and S.Das, "Implementation of reactive power-based MRAS for sensorless speed control of brushless doubly fed reluctance motor drive," IET Power Electronics, vol. 11, no. 1, pp. 192-201, Feb. 2018.

[11] M.Kumar, S.Das and K.Kiran, "Sensorless speed estimation of brushless doubly-fed reluctance generator using active power based MRAS," IEEE Trans. Power Electron., vol. 34, no. 8, pp. 7878 - 7886, Aug.2019.

[12] Y.Zhang and J.Zhu, "Direct torque control of permanent magnet synchronous motor with reduced torque ripple and commutation frequency," IEEE Trans. Power Electron., vol. 26, no. 1, pp. 235-248, 2011.

[13] J.Rodriguez, J.Pontt, C.Silva, P.Correa, P.Lezana, P.Cortes and U.Ammann, "Predictive current control of a voltage source inverter," IEEE Trans. Ind. Electron., vol. 54, no. 1, pp. 495-503, Feb.2007.

[14] H.Young, M.Perez and J.Rodriguez, "Analysis of finite-control-set model predictive current control with model parameter mismatch ina three-phase inverter," IEEE Trans. Ind. Electron., vol. 63, no. 5, pp. 3100-3107, May 2016.

[15] J.Rodriguez and P.Cortes, Predictive control of power converters and electrical drives, Valparasio, Chile: A John Wiley & Sons Ltd., 2012.

[16] M.Moazen, R.Kazemzadeh and M.-R.Azizian, "Model-based predictive direct power control of brushless doubly fed reluctance generator for wind power applications," Alexandria Engineering Journal, vol. 55, no. 3, p. 2497–2507, Sep. 2016.

[17] E.Fuentes, J.Rodrigues, C.Silva, S.Diaz and D.Quevedo, "Speed control of a permanent magnet synchronous motor using predictive current control," in Proc. IEEE International Power Electronics and Motion Control Conference (IPEMC), Wuhan, China, 17-20 May 2009.

[18] H.-T.Moon, H.-S.Kim and M.-J.Youn, "A discrete-time predictive current control for PMSM," IEEE Trans. Power Electron., vol. 18, no. 1, pp. 464-472, Jan. 2003.

[19] F.Wang, X.Mei, P.Tao, R.Kennel and J.Rodriguez, "Predictive field- oriented control for electric drives," Chinese Journal of Electrical Engineering, vol. 3, no. 1, pp. 73-78, June 2017.

[20] F.Wang, S.Li, X.Mei, W.Xie, J.Rodríguez and R.Kennel, "Model-based predictive direct control strategies for electrical drives: an experimental evaluation of PTC and PCC methods," IEEE Trans. Ind. Informat., vol. 11, no. 3, pp. 671-681, June 2015.

[21] M.Mossa and S.Bolognani, "Effective model predictive current control for a sensorless IM drive," in Proc. IEEE International Symposium on Sensorless Control for Electrical Drives (SLED), Catania, Italy, 18-19 Sept. 2017.

[22] A.Darba, F.Belie, P.D'haese and J.Melkebeek, "Improved dynamic behavior in BLDC drives using model predictive speed and current control," IEEE Trans. Ind. Electron., vol. 63, no. 2, p. 728–740, Feb. 2016.

[23] Y.Zhang, D.Xu, J.Liu, S.Gao and W.Xu, "Performance improvement of model predictive current control of permanent magnet synchronous motor drives," IEEE Trans. Ind. Appl., vol. 53, no. 4, pp. 3683 - 3695, July-Aug. 2017.

[24] S.Carpiuc and C.Lazar, "Fast real-time constrained predictive current control in permanent magnet synchronous machine-based automotive traction drives," IEEE Trans. Transport.

Electrif., vol. 1, no. 4, p. 326– 335, Dec. 2015.

[25] Y.Zhang and H.Yang, "Model predictive torque control of induction motor drives with optimal duty cycle control," IEEE Trans. Power Electron., vol. 29, no. 12, pp. 6593-6603, 12 Dec. 2014.

[26] K.Kiran, S.Das and D.Singh, "Model predictive field oriented speed control of brushless doubly-fed reluctance motor drive," in Proc. International Conference on Power, Instrumentation, Control and Computing (PICC), Thrissur, India, 18-20 Jan. 2018.

[27] Y.Zhang, J.Zhu and W.Xu, "Analysis of one step delay in direct torque control of permanent magnet synchronous motor and its remedies," in Proc. International Conference on Electrical Machines and Systems (ICEMS), Incheon, South Korea, 10-13 Oct. 2010.

[28] S.Chapra and R.Canale, Numerical methods for engineers, New York: 6th ed. McGraw-Hill Higher Education, 2010.